Environmental Science & Technology

Article

pubs.acs.org/est

Kinetics of Calcium Phosphate Nucleation and Growth on Calcite: Implications for Predicting the Fate of Dissolved Phosphate Species in Alkaline Soils

Lijun Wang,*[,†] Encarnación Ruiz-Agudo,[‡] Christine V. Putnis,*[,§] Martina Menneken,[§] and Andrew Putnis[§]

[†]College of Resources and Environment, Huazhong Agricultural University, Wuhan 430070, China

[‡]Department of Mineralogy and Petrology, University of Granada, Granada 18071, Spain

[§]Institut für Mineralogie, University of Münster, 48149 Münster, Germany

Supporting Information

ABSTRACT: Unraveling the kinetics of calcium orthophosphate (Ca−P) precipitation and dissolution is important for our understanding of the transformation and mobility of dissolved phosphate species in soils. Here we use an in situ atomic force microscopy (AFM) coupled with a fluid reaction cell to study the interaction of phosphate-bearing solutions with calcite surfaces. We observe that the mineral surface-induced formation of Ca−P phases is initiated with the aggregation of clusters leading to the nucleation and subsequent growth of Ca−P phases on calcite, at various pH values and ionic strengths relevant to soil solution conditions. A significant decrease in the dissolved phosphate concentration occurs due to the promoted nucleation of Ca−P phases on calcite surfaces at elevated phosphate concentrations and more significantly at high salt concentrations. Also, kinetic data analyses show that low concentrations of citrate caused an increase in the nucleation rate of Ca−P phases. However, at higher concentrations of citrate, nucleation acceleration was reversed with much longer induction times to form Ca−P nuclei. These results demonstrate that the nucleation-modifying properties of small organic molecules may be scaled up to analyze Ca−P dissolution−precipitation processes that are mediated by a more complex soil environment. This in situ observation, albeit preliminary, may contribute to an improved understanding of the fate of dissolved phosphate species in diverse soil systems.

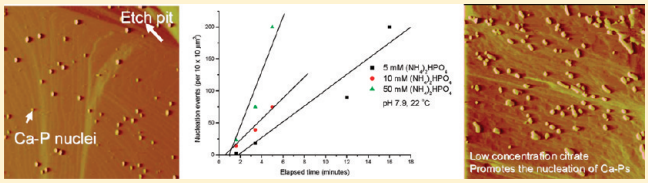

INTRODUCTION

Phosphorus (P) is an essential nutrient required for plant growth and it is also defined as 'the disappearing nutrient' due, in part, to the potential shortage of phosphate rock resources and a faster growth in demand for phosphate-based fertilizers.[1] Calcium orthophosphate (Ca−P) is the most ubiquitous form of P among the geological phosphate-bearing minerals.[2] Various components, structures, crystal phases, and hydration states of phosphates are present in soils as a result of P fertilizer application. Precipitation of soluble P in soil solutions and/or on mineral surfaces involves the formation of metastable intermediate precursor phases such as amorphous Ca−P (ACP) and brushite (DCPD) followed by the transformation to the least soluble, hydroxyapatite ($Ca_{10}(PO_4)_6(OH)_2$, HAP), as the thermodynamically stable phase of the final product in neutral to alkaline environments.[3] P present as HAP, as well as other solid phases including octacalcium phosphate (OCP) and tricalcium phosphate (TCP), is much less bioavailable to plant uptake than dissolved P species.[4] The recognition that total soil P concentration is a poor predictor of the P bioavailability has led to extensive research on chemical speciation of P in soils with the emphasis on predicting its bioavailability.[5]

It is well established that citrate is the dominant carboxylate-bearing organic molecule released by plant roots to enhance the soluble P concentration under P deficient conditions.[6,7] Moreover, alkaline soils, subjected to long-term organic additives, have been shown to accumulate substantial quantities of P in plant-available forms,[8,9] and the sorption capacities of soils for P are reduced by organic additives.[10] Despite much evidence, understanding the chemical nature of organic molecules, especially low molecular weight organic acids and their influences on P mobility in soil solutions, remains limited.

Calcite is a common mineral and constituent of sediments and phosphate can both adsorb on and desorb from calcite surfaces.[11] Thus, calcite can serve as both a source and sink of phosphate in alkaline soils, thereby influencing the fate of phosphate. The interactions between soluble orthophosphates and calcite have been extensively studied, both as a novel method of apatite synthesis[12] and also because of the frequent occurrence of soil systems rich in calcite and the dominant effect of calcite on phosphate solubility.[13] It is evident that surface adsorption/reaction and subsequent precipitation are major mechanisms of P immobilization (precipitation) in

Received: August 21, 2011
Revised: November 30, 2011
Accepted: December 5, 2011
Published: December 5, 2011

calcite-rich alkaline soils,[14,15] lowering its bioavailability when dissolved P is added as a fertilizer. Until recently, physical models for the interactions between dissolved P species and the components of calcareous soils as well as the binding to phosphate in soil, water, and sediments, which determine the bioavailability and mobility of phosphate, were derived largely from macroscopic investigations of sorption isotherms and surface complexation modeling.[16−19] However, there is still a lot of uncertainty and variation among these macroscopic experiments. In this study, we investigate, by a direct microscopic observation, the Ca−P nucleation and subsequent growth on calcite surfaces in the absence and presence of citrate using in situ atomic force microscopy (AFM) coupled with a fluid reaction cell through which flowed solutions with varying compositions relevant to soil solution conditions. To our knowledge, there has been no experimental effort to directly measure the thermodynamic and kinetic contributions to the surface nucleation rates of Ca−P phases on calcite under chemical conditions that mimic natural phosphate dissolution−precipitation environments. These direct observations may be relevant to the previously unrecognized relationship that rationalizes recently reported results showing P dynamics in the soil-plant continuum,[20] especially in the rhizosphere enriched in various low molecular weight organic acids.

EXPERIMENTAL SECTION

In situ dissolution experiments were performed using a Digital Instruments Nanoscope IIIa AFM working in contact mode and equipped with a fluid cell. Prior to each experiment a rhombohedral calcite crystal of optical quality Iceland Spar (Chihuahua, Mexico) was cleaved in order to expose a fresh cleavage surface ($10\bar{1}4$). The concentrations of diammonium phosphate, $(NH_4)_2HPO_4$ solutions ranged from 5 to 50 mM and passed through the fluid cell. Additionally, NaCl at concentrations ranging from 0.01 to 0.5 M was added to the phosphate solutions to study the effects of ionic strength. Also monosodium citrate (1−10 μM) was added to the phosphate solution to observe the effect of an organic additive. The pH values of $(NH_4)_2HPO_4$ solution in the absence and presence of different citrate concentrations were adjusted to pH 7.9 or pH 8.8 using 0.01 M NaOH. The chosen flow rate was to ensure surface-controlled reaction rather than diffusion control.[21] Etch pit spreading rates during dissolution were determined for each concentration of phosphate solution.[21]

The PHREEQC program[22] was used to calculate surface and solution speciation with increasing calcite dissolution into a 40 μL volume of phosphate-bearing solution in the AFM fluid cell in our experiments. Following the dissolution experiments, reacted crystals were analyzed using a HORIBA Jobin Yvon HR800 micro-Raman spectrometer (the excitation line of 633 nm of a He−Ne laser) to detect any possible new phases formed on calcite.

RESULTS

Dissolution Features on Calcite ($10\bar{1}4$) Cleavage Surfaces. Prior to the input of reaction solutions, the calcite ($10\bar{1}4$) cleavage face was exposed to deionized water (pH 6.0). Dissolution immediately occurred with the formation of typical rhombohedral etch pits on the exposed surfaces (Figure 1A). These were used to establish the crystallographic orientation of the seed substrates. The average movement velocity of etch pits, v_{sum}, (i.e., the rate of change in etch pits length along $[\bar{4}41]$ or $[48\bar{1}]$, sum of the retreat velocity of the acute and obtuse steps, $v_+ + v_-$) was about 2.0 nm/s in deionized water (pH 6.0). The pit spreading rate decreased rapidly in the pH range of 3−5, from 13 ± 1 nm/s (n = 3) at pH 3.9 to 5 ± 1 nm/s (n = 3) at pH 5.1 (Figure 2A). Above pH 6.0, the pit spreading rate slightly decreased, from 1.7 ± 0.3 nm/s (n = 4) at pH 7.1, to 1.5 ± 0.4 nm/s (n = 3) at pH 7.8, and to 1.3 ± 0.2 nm/s (n = 3) at pH 9.6 (Figure 2A).

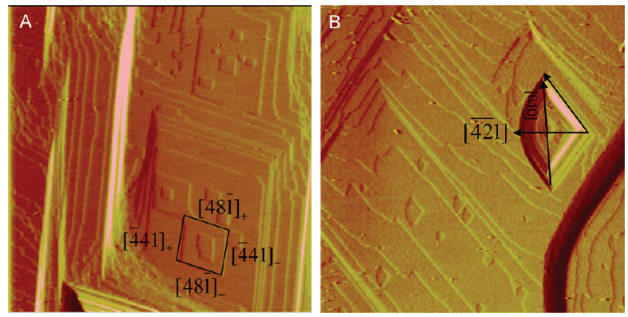

Figure 1. Calcite dissolution in (A) water at pH 6.0 (rhombohedral etch pits) and in (B) 10 mM $(NH_4)_2HPO_4$ solution at pH 8.8 (fan-shaped etch pits). Because of the rhombohedral symmetry ($R\bar{3}2/c$) of calcite, the etch pits on the $\{10\bar{1}4\}$ faces developed in water are bounded by the $[\bar{4}41]$ and $[48\bar{1}]$ vectors that are related by the only symmetry element, a c-glide plane, perpendicular to this surface. Fan-shaped pits formed on calcite upon the input of $(NH_4)_2HPO_4$ solution. Images A and B, 10 × 10 μm.

In the presence of $(NH_4)_2HPO_4$, the etch pits changed from the characteristic rhombohedral morphology to triangular- or even fan-shaped (Figure 1B). Values of etch pit retreat rates along the $[\bar{4}21]$ diagonal or along the [010] diagonal were measured, and the pit retreat rate of v_{sum} in the presence of 5, 10, or 50 mM $(NH_4)_2HPO_4$ at constant pH 7.9 remained similar or slightly increased to 2.1 ± 0.3 (n = 3), 2.3 ± 0.3 (n = 3), and 2.6 ± 0.5 nm/s (n = 4), respectively compared to that in pure water (2.0 ± 0.4 (n = 6), pH 6.0) (Figure 2B). When NaCl (0.01, 0.1, or 0.5 M) was introduced into 50 mM $(NH_4)_2HPO_4$ solution (pH 7.9), the rate of pit retreat increased to 2.8 ± 0.4 (n = 4), 3.4 ± 0.3 (n = 4), and 5.1 ± 0.4 (n = 3) nm/s, respectively (Figure 2C). Also, an increase in etch pit density with increasing NaCl concentration was observed (Figure 4 A and B).

Calcium Phosphate Nucleation on Calcite ($10\bar{1}4$) Cleavage Surfaces in the Absence and Presence of Citrate. The dissolution of calcite in the presence of all experimental phosphate solutions resulted in nucleation of Ca−P nanoparticles on the calcite surfaces, possibly through a Ca−P precursor phase transformed to apatite as identified by ex-situ Raman spectroscopy (discussed later). Figure 3A shows typical Ca−P particles formed on calcite ($10\bar{1}4$) surfaces. The average height of initially formed nuclei was only about 1.2 nm (Circle 1 in Supporting Information (SI) Figure S1), and the growing clusters ranged from 2.4 to 3.9 nm in height (Circle 2 in SI Figure S2). The number of Ca−P nuclei increased linearly with time for a given phosphate concentration, and faster nucleation rates were observed with increasing the $(NH_4)_2HPO_4$ solution concentration when the solution pH was kept constant (pH 7.9) (Figure 3B), whereas the nucleation rate significantly decreased when the pH was raised to 8.8 (Figure 3C). Moreover, as seen by comparing Figure 4A with Figure 4C, the calcite surface displayed a greater density of Ca−P nuclei after

dx.doi.org/10.1021/es202924f | Environ. Sci. Technol. 2012, 46, 834−842

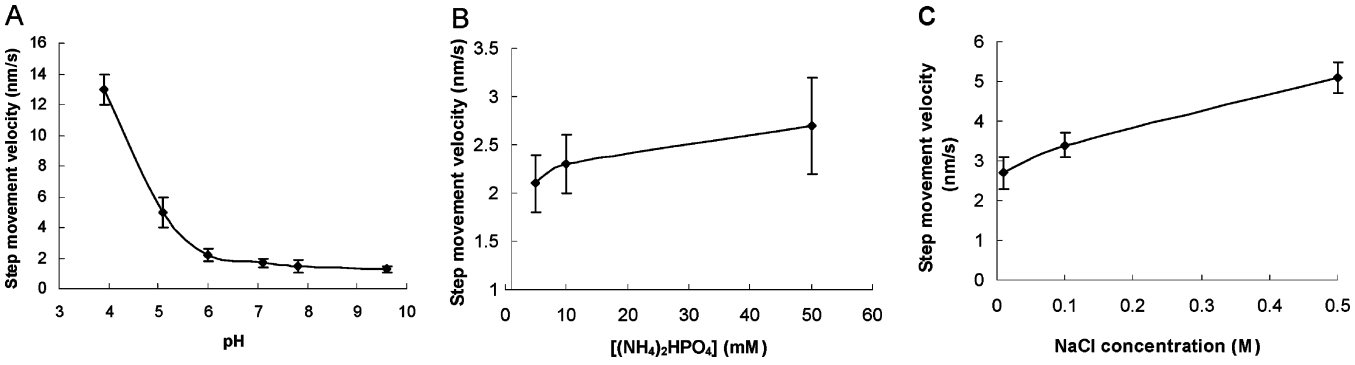

Figure 2. Retreat velocity of etch pits on calcite $(10\bar{1}4)$ surfaces under various experimental conditions. (A) A range of pH values, (B) $(NH_4)_2HPO_4$ concentrations at pH 7.9 (*IS* = 0.014, 0.028, or 0.144 M at 5 mM, 10 mM, or 50 mM $(NH_4)_2HPO_4$, respectively), and (C) NaCl concentrations with constant concentration 50 mM $(NH_4)_2HPO_4$ at pH 7.9 (*IS* = 0.153, 0.242, or 0.654 M, respectively, at 0.01 M NaCl + 50 mM $(NH_4)_2HPO_4$, 0.1 M NaCl + 50 mM $(NH_4)_2HPO_4$, or 0.5 M NaCl + 50 mM $(NH_4)_2HPO_4$, respectively).

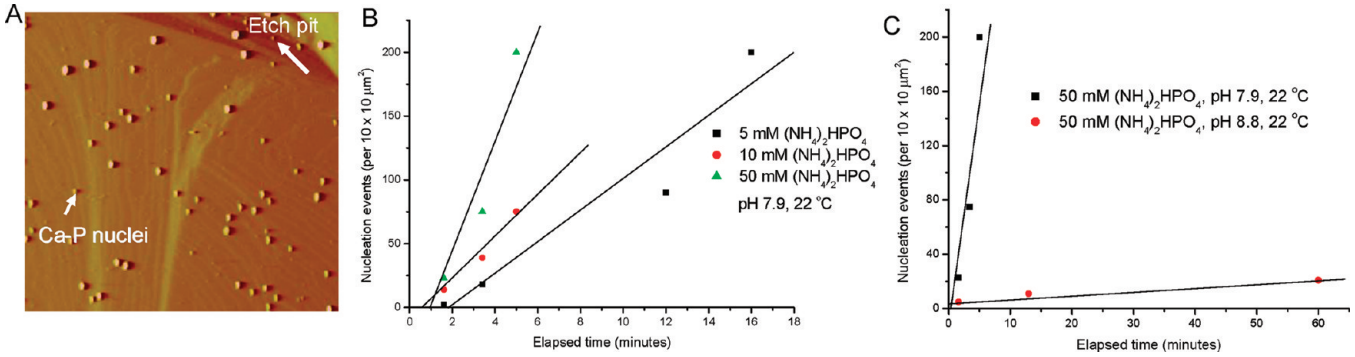

Figure 3. Kinetic analysis of surface nucleation of Ca−P phases on calcite substrates. (A) AFM image of Ca−P particles on a calcite surface during in situ nucleation events. Image 10 × 10 μm. (B) Plot against time of different concentrations of $(NH_4)_2HPO_4$ and (C) pH values.

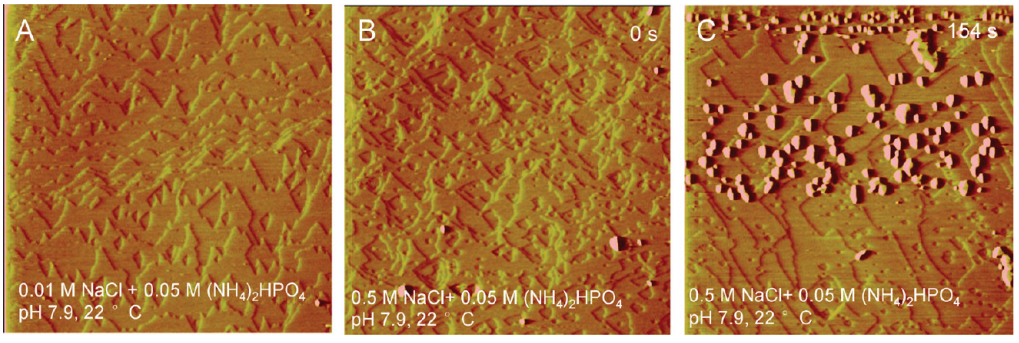

Figure 4. AFM deflection images of calcite surfaces dissolving in aqueous solutions of $(NH_4)_2HPO_4$ with (A) low salt (0.01 M NaCl), (B) high salt (0.5 M NaCl), and (C) high salt-induced rapid nucleation of Ca−P particles (image taken 154 s after injection of 0.5 M NaCl and 50 mM $(NH_4)_2HPO_4$ at pH 7.9, T = 22 °C). Note the high etch pit density attained at 0.5 M NaCl. Images A−C, 10 × 10 μm.

injecting 50 mM $(NH_4)_2HPO_4$ solution with 0.5 M NaCl than the solution with 0.01 M NaCl (Figure 4C).

Upon input of a 50 mM $(NH_4)_2HPO_4$ solution in the presence of 1 μM citrate (pH 7.9), greater nucleation rates were observed than in the absence of citrate (Figure 5A and B). The growth of the nucleated particles led to the formation of 1-D short chains after 281 s reaction time (shown by arrows in Figure 5C and D), and 2-D plates after 375 s reaction time (shown by dotted circle in Figure 5D). When the citrate concentration was raised to 10 μM, the Ca−P nucleation was inhibited as no further precipitation was seen under AFM (Figure 5E−G).

Calcium Phosphate Growth and Dissolution on Calcite $(10\bar{1}4)$ Cleavage Surfaces. Following nucleation, these Ca−P nanoparticles were well-attached to the surface and grew when neighboring particles came into contact and coalesced into 1-D chains (shown by an arrow in Figure 6A). When the scanning AFM tip was lifted for 3 h, a further diffusion-controlled growth leading to the formation of 2-D plates was observed at concentration 50 mM of $(NH_4)_2HPO_4$ (Figure 6B and C). The height of the initially formed Ca−P plates on calcite was about 2.3 nm (SI Figure S2). The newly formed layers were characterized using Raman spectroscopy. A strong and symmetric peak at 1086 cm^{-1} corresponds to the characteristic spectrum of the calcite substrate (the stretching vibration (υ_1 mode) of CO_3), and two visibly weaker peaks at 960 and 430 cm^{-1} can be assigned to υ_1PO_4 and υ_2PO_4 (carbonated Ca−P in an apatite lattice), respectively. However,

dx.doi.org/10.1021/es202924f | *Environ. Sci. Technol.* 2012, 46, 834−842

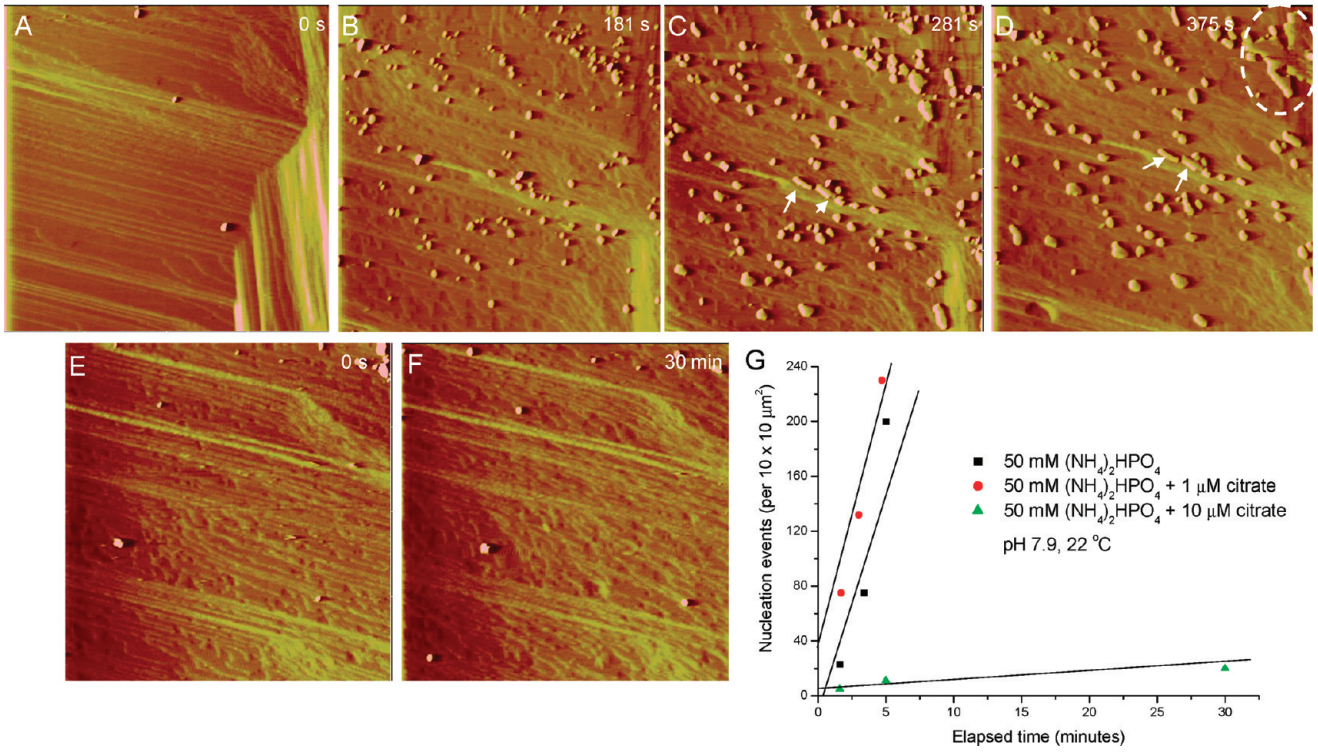

Figure 5. Nucleation kinetics of Ca−P phases on calcite in the presence of (A-D) 1 μM citrate and (E and F) 10 μM citrate with 50 mM $(NH_4)_2HPO_4$ at pH 7.9. (G) Plot showing linear scaling of surface nucleation with time and dependence of the nucleation rate given by slopes of the lines. AFM Images A-F, 10 × 10 μm.

these two peaks are significantly broadened, suggesting that metastable phases such as ACP or poorly crystalline HAP may exist (Figure 6D). This can be further confirmed by observing the dissolution behavior of these newly forming layers. Upon introduction of doubly deionized water into the fluid cell, the top layers of the new Ca−P phase formed on the calcite surfaces (Figure 6C) rapidly dissolved within minutes (Figure 7A−C), and nanoparticles were formed after 19 min dissolution reaction time, becoming smaller after 25 min of further dissolution (Figure 7D−F), indicating that the new phase (loose aggregates) is quite unstable in water.

DISCUSSION

The dissolution of calcite in the presence of all phosphate solutions provided a reliable source of Ca^{2+} ions, which resulted in nucleation and growth of a Ca−P phase on the dissolving calcite surface. Based on our PHREEQC simulations, a Ca−P phase is thermodynamically favorable to crystallize on calcite in the AFM fluid cell conditions. The relative supersaturation for forming Ca−P phases can be expressed by

$$\sigma = \frac{\mathrm{IAP}}{K_{sp}} - 1 = S - 1 \tag{1}$$

where IAP is the actual ion activity product and K_{sp} is its value at equilibrium (the solubility product for a given phase, $-\log(K_{sp,\ HAP})$ = 116.8 for HAP at 25 °C),[3] and S is the supersaturation ratio. Thus, for HAP,

$$S = \frac{[a(Ca^{2+})]^{10}[a(PO_4^{3-})]^6[a(OH^-)]^2}{K_{sp}} \tag{2}$$

where a is the activity of the Ca^{2+}, PO_4^{3-} or OH^- ion. Saturation index is defined as SI = log (S). When $S > 1$, the solution is supersaturated and the mineral may nucleate and grow. For surface nucleation events, spontaneous crystallization does not occur until critical conditions are reached and the driving force S is sufficiently high. Rather, a metastable equilibrium condition persists during an "induction period", τ, prior to crystal formation. If the simplifying assumption is made that τ is essentially concerned with classical nucleation, then we can use eq 3[23]

$$\ln \tau \propto \left[C_1 + C_2 \frac{\gamma_{SL}^3}{k_B^3 T^3 (\ln S)^2} \right] \tag{3}$$

in which C_1 and C_2 are independent constants, γ_{SL} is the interfacial free energy between the mineral surfaces (s) and the liquid (L), and k_BT is the product of the Boltzmann constant and the system temperature.

In experiments to examine the effect of ionic strength on calcite dissolution, we adjusted the solution composition by adding NaCl as background electrolyte to the 50 mM $(NH_4)_2HPO_4$ solution, which changed ionic strength (IS = $0.5\sum_i^n c_i z_i^2$, where z_i and c_i represent the ionic charge and concentration of the "i^{th}" species, respectively). Ionic strength, in turn, may influence the step speed by changing the activity coefficients of ions in solution. This depends on anions/cations from background electrolytes. These changes were treated using the Davies equation:

$$-\log(\gamma_i) = \frac{Az_i^2\sqrt{I}}{1+\sqrt{I}} - 0.3I \tag{4}$$

where A is a Debye−Hückel constant.[24]

dx.doi.org/10.1021/es202924f | Environ. Sci. Technol. 2012, 46, 834−842

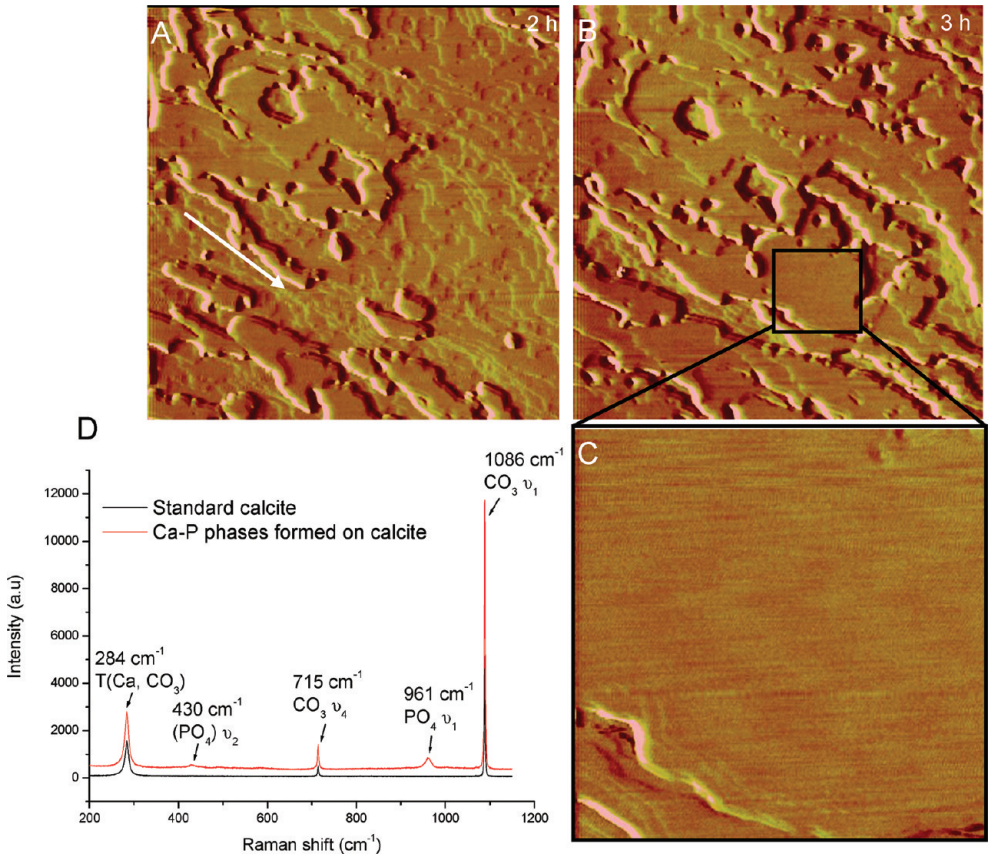

Figure 6. Ca–P phase growth on calcite. (A) Nucleated particles come into contact and coalesce into 1-D chains (shown by an arrow), and (B) a further growth into 2-D plates was observed after injecting 50 mM $(NH_4)_2HPO_4$ solution and the AFM tip was lifted for 3 h. (C) High-resolution AFM image (in the black rectangle marked in Figure 6B) showing a very flat 2-D plate. (D) Raman spectra of the 2-D plates and calcite standard, demonstrating the presence of an apatite phase. Images A and B, 10 × 10 μm; C, 2 × 2 μm.

In the present study, velocities of etch pit retreat (Figure 2C) and pit density (Figure 4A and B) in $(NH_4)_2HPO_4$ solutions with NaCl were significantly higher than in the same solutions without NaCl. Net increase in the overall dissolution rates depends on retreat and deepening rates as well as the nucleation density of etch pits.[21] In our experiments, no significant deepening of the calcite surface exposed to the experimental solution was observed. Therefore, differences in dissolution rates in the absence and presence of NaCl result from changes in etch pit nucleation density and/or retreat rates. Previous AFM studies demonstrated that background electrolytes enhance the calcite dissolution rate,[21] and the magnitude of this enhancement is determined by the nature and concentration of the electrolytes through modifying water structure dynamics as well as solute and surface hydration.[25] At relatively high ionic strength, Cl^- ions determine the solvent structure around Ca^{2+} and calcium removal from the surface structure, the rate limiting step for dissolution. Moreover, a high concentration of Cl^- ions (0.5 M) increases the etch pit density. This can be explained by the disruption of surface hydration water at the calcite surface.[21] Furthermore, the distribution of surface-active ions determines the calcite dissolution rates at various pH (Figure 2A): H^+ at pH 2–5, HCO_3^- at pH 5–8, and OH^- at pH >10.[26,27]

For all initial phosphate concentrations a rapid sorption of phosphate on calcite was observed, based on morphology changes of the etch pits captured immediately following the addition of $(NH_4)_2HPO_4$ solution into the AFM fluid cell (Figure 1B). Rapid sorption of phosphate on calcite has previously been reported.[28] When $(NH_4)_2HPO_4$ solutions were replaced by phosphate-free water solution, desorption of phosphate from the calcite surface was also found to be fast: the modified etch pits immediately returned to their original morphology, the rhombohedral form (Figure 1A). The sorption reversibility suggests that phosphate may not be incorporated into the calcite crystal lattice under the present experimental conditions even at higher phosphate concentrations. In addition, phosphate adsorption is also pH-dependent, suggesting that some specific phosphate species are preferentially adsorbed.[17]

A proposed surface complexation model (SCM) for the calcite-water interface suggests that two primary hydration sites with a 1:1stoichiometry, $>CaOH^0$ and $>CO_3H^0$ exist on the $(10\bar{1}4)$ face (the notation ">" means surface sites).[29–31] According to this model, the complexes formed from the primary species exposed to the aqueous solution include: $>CO_3^-$ and $>CO_3Ca^+$ at the $>CO_3$ sites; $>CaCO_3^-$, $>CaOH_2^+$ and $>CaHCO_3^0$ at the >Ca sites. In this study, we used the notation and values of complexation constants for reactions on the calcite surface[17,30] (See Supporting Information Table S1). In the reaction solution containing 50 mM $(NH_4)_2HPO_4$ at pH 7.9, phosphate primary speciation in solution is dominated by HPO_4^{2-} and $H_2PO_4^-$, whereas the concentration of PO_4^{3-} is very low (8.3×10^{-6} M) according to our PHREEQC calculations. Phosphate adsorbs onto the >Ca sites to mainly form

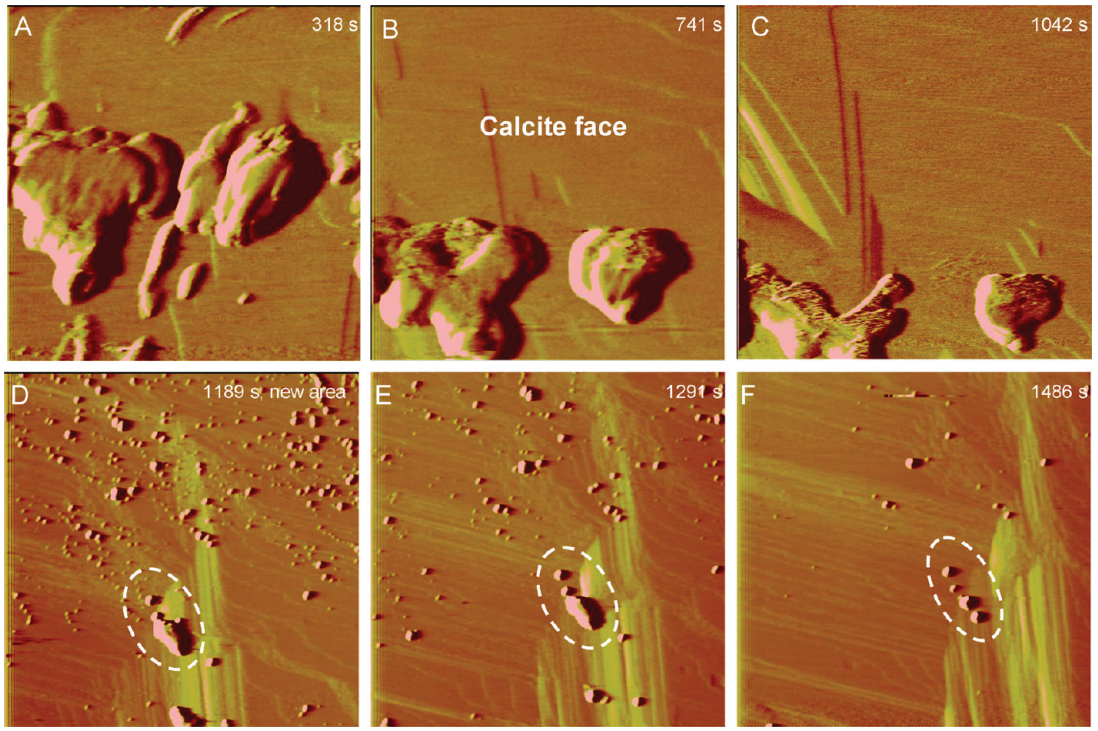

Figure 7. AFM images showing the dissolution of the newly forming Ca−P phase on calcite after injecting pure water. (A−C) The Ca−P layers dissolved quickly, and (D−F) nanoparticles were formed at 19 min dissolution reaction and became smaller following 25 min dissolution shown by white dotted circles. Images A-C, 2 × 2 μm; D-F, 10 × 10 μm.

>sCaHPO$_4^-$ and >CaHPO$_4^-$, and their concentrations are 2.9 × 10^{-7} and 1.6 × 10^{-8} mol m^{-2}, respectively.

In addition to phosphate species adsorbed on calcite, organic ligands can also attach to the dissolving calcite surfaces. Calcite dissolution is controlled by the hydrolysis of calcite centers (>CaOH$_2^+$) at pH > 6.[32] The presence of organic ligands such as citrate can influence calcite dissolution rates by changing its surface composition. The dominant Ca species, >CaOH$_2^+$ on the calcite surface at 6 < pH < 11 can react with an organic ligand (L^{-m}) through the following reaction:[33]

$$>\mathrm{CaOH_2^+} + \mathrm{L}^{-m} = \mathrm{CaL}^{1-m} + \mathrm{H_2O} \qquad (5)$$

Therefore, ligand promoted dissolution rates are proportional to the >CaL^{1-m} surface complex concentration.[34]

In the present study, the presence of 1 μM, 5 μM, 10 μM, or 1 mM citrate (at pH 7.5) increased the retreat velocities of etch pits to 4.3 ± 0.8 (n = 3), 4.0 ± 0.7 (n = 6), 4.2 ± 0.8 (n = 3), and 5.0 ± 0.3 nm/s (n = 3), respectively. This suggests that citrate can enhance calcite dissolution when compared to the rates in pure water (about 2 nm/s). A very recent study of bulk measurements of calcite dissolution rates also show a significant increase with increasing the citrate concentration.[33] Surprisingly, at relatively high concentration (10 μM) citrate dramatically inhibits nucleation of Ca−P phases (Figure 5E and F), though the velocity of etch pit retreat remains almost constant between 1 and 10 μM for citrate. By contrast, an increase in nucleation rates of Ca−P phases on calcite in the presence of low concentration citrate (1 μM) was observed (Figure 5A−D).

Citrate, a carboxylate-rich molecule (HOC(COOH)-(CH$_2$COOH)$_2$), interacts with mineral surfaces to influence both the crystal morphologies and growth rates.[35,36] The addition of citrate may also decrease the saturation state of precipitating Ca−P minerals by the formation of metal and P organic complexes in aqueous solution, and the influence of citrate on mineral solubility may explain the inhibition at high citrate concentrations. Current thermodynamic databases are likely to be insufficient to calculate the effect of citrate on these saturation states as well as Ca−citrate complexes. Experimentally, in a DCPD-citrate system, citrate (10 μM) alters DCPD surface energies, thus delaying nucleation manifested by longer induction times.[37] eq 3 suggests that there is an increase in the interfacial tension γ_{SL} following the introduction of the same concentration of citrate (10 μM) in the present study. This results in the inhibition of the Ca−P phase formation by an increase in the induction time (presumably S is unchanged in this crystallization process) (Figure 5G). However, the interfacial free energy only captures the thermodynamic component of the nucleation barrier. Nucleation rates are also controlled by kinetic barriers associated with desolvation, hydrolysis, or other chemical reactions, binding and unbinding events, and in some cases, diffusion.[38,39]

At low concentrations, the interaction of carboxyl groups of citrate with surface Ca^{2+} ions may increase the local concentration of a carboxylated additive in the vicinity of these cations, thereby lowering the energy barrier for nucleation and inducing the precipitation of Ca−P phases, in the "modified supersaturated solutions".[40,41] Other carboxylate-bearing molecules such as aspartic acid (Asp)-rich motifs in peptides and proteins have been postulated to function by preferentially binding to cations during the controlled formation of biominerals such as calcite.[42,43] Elhadj et al. defined a systematic relationship between the ability of biomolecules enriched in Asp to promote the growth of calcite and their net negative molecular charge and hydrophilicity.[44] The rate enhancement of low concentrations of Asp-containing molecules arises from an increase in the kinetic coefficient, and

the mechanism of growth enhancement has been interpreted to be a catalytic process, whereby Asp-containing molecules reduce the magnitude of the diffusive barrier, E_K, by perturbations that displace water molecules. The result is a decrease in the energy barrier for attachment of solutes to the solid phase through cation desolvation.[44,45]

It has been shown for the Ca−P system that precursor phases including ACP, DCPD and OCP may be stabilized kinetically for certain periods of time despite the fact that the driving force for the formation of the thermodynamically most stable phase of HAP are appreciable.[3] Therefore for solutions containing 50 mM total phosphate, the precipitating phase may be any of these precursor phases. The evolution of solution composition during calcite dissolution in the presence of phosphate solutions was simulated using PHREEQC. Calculated total concentration of calcium carbonate (assuming a crystal size of ca. 3 × 3 × 1 mm) dissolved in 40 μL fluid cell in the presence of 5, 10, or 50 mM $(NH_4)_2HPO_4$ solutions at pH 7.9 in equilibrium is 1.16×10^{-3}, 1.59×10^{-3} and 3.22×10^{-3} M, respectively. When 0.1 M NaCl was added into 5, 10, or 50 mM $(NH_4)_2HPO_4$ solutions, the total concentration of calcite dissolved in each of the phosphate solutions increased to 2.48×10^{-3}, 3.89×10^{-3} and 1.21×10^{-2} M, respectively. Saturation indices (SI) of possible Ca−P phases including DCPD, OCP, and HAP calculated using Wateq4f database (Thermodynamic databases for Ca−P phases are likely to be insufficient,[46] therefore a large variation in $\log(K_{sp,\ HAP})$ in the different databases of PHREEQC may lead to different results of SI) at the last step of dissolution reaction in the presence of 50 mM $(NH_4)_2HPO_4$ solution at pH 7.9 is 1.13, 39.62, and 32.32, respectively. Following the addition of 0.1 M NaCl into 50 mM $(NH_4)_2HPO_4$ solution at pH 7.9, SI with respect to DCPD, OCP and HAP was raised to 1.72, 42.49, and 34.51, respectively. This suggests that with the increase in phosphate concentration, reaction conditions in the presence of high concentrations of NaCl are more favorable for OCP and HAP to form on calcite than at low NaCl concentrations (Figure 4C), though adsorbed phosphate decreases as the ionic strength increases due to an increase in the overall negative charge density on the negatively charged surface species ($>CaCO_3^-$ and $>CO_3^-$).[17] Consequently, the ionic strength primarily influences the activity coefficients for aqueous phosphate species in addition to its influence on calcite dissolution (Figure 2C).

If the reaction occurring in the present system was the precipitation of any known Ca−P phase, the ratio of precipitated calcium to that of phosphorus should be in the range between 1.0 and 1.67, the stoichiometric Ca/P ratios in DCPD and HAP, respectively. However, the calculated Ca/P molar ratio in our reaction solutions of 40 μL fluid cell is about 0.06, suggesting that virtually all the Ca^{2+} ions released from the dissolving calcite is taken up by the precipitating phase. The initial Ca/P ratio in solution influences both solution speciation and kinetics of incorporation (activation barriers differ for calcium and phosphate ions).[47] Experiments in supersaturated solutions containing nonstoichiometic lattice ion concentrations showed marked changes in growth rates even at the same thermodynamic supersaturation, suggesting that cation and anion attachment frequencies are proportional to the concentrations of these species only, that is, the step rate with a clear maximum in stoichiometric solutions.[48−51]

For Ca−P formation pathway on surfaces, a cluster-growth model has been proposed and debated for many years.[52,53] Our AFM observations clearly show that the nucleation and formation of Ca−P crystals on a calcite mineral surface proceed through a multistage process that involves the occurrence and aggregation of clusters. The cluster aggregates that are in contact with the dissolving surfaces of calcite start to coalesce and form nanoparticles (Circle 2 in SI Figure S1) by a closer packing of the clusters. These nanoparticles further grow and develop to yield spheroidal particles with diameters of ∼100−200 nm (Figure 5B) which subsequently form 1-D chains along the step edges (Figures 5C and 6A), and finally 2-D plates (Figures 5D and 6C). The spheroidal morphology of the Ca−P phase is typical for crystals grown in the presence of high carbonate concentration.[54] A similar surface-induced apatite crystallization process was captured using a Langmuir monolayer of arachidic acid $[CH_3(CH_2)_{18}COOH]$ serving as the nucleation template.[55]

Collectively, the distribution of phosphate at the calcite-water interface is dependent on the solution composition, including the activity of phosphate species, pH and ionic strength, thereby influencing phosphate availability. Based on the present study, we predict a significant decrease in the dissolved phosphate concentration of the soil solution due to increased phosphate adsorption and the corresponding precipitation on mineral surfaces at elevated phosphate concentrations. The bioavailability of phosphate will be reduced even further at high salt concentrations. In addition, a large degree of sorption reversibility and instability of newly forming Ca−P phases in water (Figure 7) on calcite were observed. This may enhance the availability of phosphate, where a decrease in the aqueous phosphate concentration (possibly from plant root uptake or even irrigation) might lead to release of phosphate from the calcite surface. Furthermore, based on the mean citrate concentration in the rhizosphere (higher than the concentration, 10 μM, used in our AFM experiments), citrate can increase P availability by suppressing crystallization of Ca−P phases such as HAP.

Our results provide a preliminary understanding of mineral surface-induced Ca−P formation, with possible implications for the management of phosphate precipitation/dissolution in soils. In addition, these direct AFM observations and the kinetic analyses may be applied to predict the behavior of more soluble forms of phosphate entering freshwater systems, and thereby exhibiting the inseparable link between the chemical species of phosphate and the potential for phosphate-induced eutrophication.[56]

■ ASSOCIATED CONTENT

Ⓢ Supporting Information

Experimental details; Analysis of calcite dissolution reactions; Surface complexation reactions in the presence of phosphate and their stability constants at the calcite-solution interface (Table S1); AFM images of initially forming nuclei and subsequent 2-D plates of Ca−P phases (Figures S1 and S2); Supporting references. This material is available free of charge via the Internet at http://pubs.acs.org.

■ AUTHOR INFORMATION

Corresponding Author

*Phone/Fax: +86-27-87288095 (L.W.); +49-251-8333454 (C.V.P.). Fax: +49-251-8338397 (C.V.P.). E-mail: ljwang@mail.hzau.edu.cn (L.W.); putnisc@uni-muenster.de (C.V.P.).

■ ACKNOWLEDGMENTS

This work was supported in part by the National Natural Science Foundation of China (Grant No. 41071208) and a startup grant from the Huazhong Agricultural University (52204-09008) to Lijun Wang. E.R.-A. acknowledges a reintegration grant from the University of Granada (Plan Propio program). Experimental facilities in the Institut für Mineralogie, Münster are supported by the Deutsche Forschungsgemeinschaft (DFG). We also thank Dr. Thorsten Geisler (University of Bonn, Germany) for constructive suggestions for the Raman assignment of Ca−P phases. We also thank the reviewers for positive and helpful comments for the improvement of the manuscript.

■ REFERENCES

(1) Gilbert, N. The disappearing nutrient. *Nature* **2009**, *461*, 716−718.
(2) Filippelli, G. M. The global phosphorous cycle: Past, present, and future. *Elements* **2008**, *4*, 89−95.
(3) Wang, L. J.; Nancollas, G. H. Calcium orthophosphates: Crystallization and dissolution. *Chem. Rev.* **2008**, *108*, 4628−4669.
(4) Wang, L. J.; Lu, J. W.; Xu, F. S.; Zhang, F. S. Dynamics of crystallization and dissolution of calcium orthophosphates at the near-molecular level. *Chin. Sci. Bull.* **2011**, *56*, 713−721.
(5) Traina, S. J.; Laperche, V. Contaminant bioavailability in soils, sediments, and aquatic environments. *Proc. Natl. Acad. Sci. U.S.A.* **1999**, *96*, 3365−3371.
(6) Dinkelaker, B.; Römheld, V.; Marschner, H. Citric acid excretion and precipitation of calcium in the rhizosphere of white lupin (*Lupinus albus* L.). *Plant Cell Environ.* **1989**, *12*, 285−292.
(7) Keerthisinghe, G.; Hocking, P. J.; Ryan, P. R.; Delhaize, E. Effect of phosphorus supply on the formation and function of proteoid roots of white lupin. *Plant Cell Environ.* **1998**, *21*, 467−478.
(8) von Wandruszka, R. Phosphorus retention in calcareous soils and the effect of organic matter on its mobility. *Geochem. Trans* **2006**, *7*, 6 DOI: 10.1186/1467-4866-7-6.
(9) Whalen, J. K.; Chang, C. Phosphorus accumulation in cultivated soils from long-term annual applications of cattle feedlot manure. *J. Environ. Quality* **2001**, *30*, 229−237.
(10) Iyamuremye, F.; Dick, R. P.; Braham, J. Organic amendments and phosphate dynamics: II. Distribution of soil phosphorus fractions. *Soil Sci.* **1996**, *161*, 436−443.
(11) Suzuki, T.; Inomata, S.; Sawada, K. Adsorption of phosphate on calcite. *J. Chem. Soc. Faraday Trans.* **1986**, *82*, 1733−1743.
(12) Kasioptas, A.; Geisler, T.; Perdikouri, C.; Trepmann, C.; Gussone, N.; Putnis, A. Polycrystalline apatite synthesised by hydrothermal replacement of calcium carbonates. *Geochim. Cosmochim. Acta* **2011**, *75*, 3486−3500.
(13) Avnimelech, Y. Calcium-carbonate-phosphate surface complex in calcareous systems. *Nature* **1980**, *288*, 255−257.
(14) House, W. A.; Donaldson, L. Adsorption and coprecipitation of phosphate on calcite. *J. Colloid Interface Sci.* **1986**, *112*, 309−324.
(15) Hinedi, Z. R.; Goldberg, S.; Chang, A. C.; Yesinowski, J. P. A ^{31}P and ^{1}H MAS NMR study of phosphate sorption onto calcium carbonate. *J. Colloid Interface Sci.* **1992**, *152*, 141−160.
(16) Milero, F.; Huang, F.; Zhu, X.; Liu, X.; Zhang, J. Z. Adsorption and desorption of phosphate on calcite and aragonite in seawater. *Aquat. Geochem.* **2001**, *7*, 33−56.
(17) SØ, H. U.; Postma, D.; Jakobsen, R.; Larsen, F. Sorption of phosphate onto calcite; results from batch experiments and surface complexation modelling. *Geochim. Cosmochim. Acta* **2011**, *75*, 2911−2923.
(18) Devau, N.; Le Cadre, E.; Hinsinger, P.; Jaillard, B.; Gérard, F. Soil pH controls the environmental availability of phosphorus: Experimental and mechanistic modelling approaches. *Appl. Geochem.* **2009**, *24*, 2163−2174.
(19) Devau, N.; Hinsinger, P.; Le Cadre, E.; Colomb, B.; Gérard, F. Fertilization and pH effects on processes and mechanisms controlling dissolved inorganic phosphorus in soils. *Geochim. Cosmochim. Acta* **2011**, *75*, 2980−2996.
(20) Shen, J. B.; Yuan, L. X.; Zhang, J. L.; Li, H. G.; Bai, Z. H.; Chen, X. P.; Zhang, W. F.; Zhang, F. S. Phosphorus dynamics: From soil to plant. *Plant Physiol.* **2011**, *156*, 997−1005.
(21) Ruiz-Agudo, E.; Kowacz, M.; Putnis, C. V.; Putnis, A. The role of background electrolytes on the kinetics and mechanism of calcite dissolution. *Geochim. Cosmochim. Acta* **2010**, *74*, 1256−1267.
(22) Parkhurst, D. L.; Appelo, C. A. J. Users guide to PHREEQC-(version 2). A computer program for speciation, batch reaction, one-dimensional transport, and inverse geochemical calculations. In *U.S. Geological Survey Water-Resources Investigations Report*, 99-4259; U.S. Geological Survey: Washington, DC, 1999.
(23) Wang, L. J.; Qiu, S. R.; Zachowicz, W.; Guan, X. Y.; De Yoreo, J. J.; Nancollas, G. H.; Hoyer, J. R. Modulation of calcium oxalate crystallization by linear aspartic acid-rich peptides. *Langmuir* **2006**, *22*, 7279−7285.
(24) Weaver, M. L.; Qiu, S.; Hoyer, J. R.; Casey, W. H.; Nancollas, G. H.; De Yoreo, J. J. Inhibition of calcium oxalate monohydrate growth by citrate and the effect of the background electrolyte. *J. Cryst. Growth* **2007**, *306*, 135−145.
(25) Stack, A. G. Molecular dynamics simulations of solvation and kink site formation at the {001} Barite-water interface. *J. Phys. Chem. C* **2009**, *113*, 2104−2110.
(26) Dolgaleva, I. V.; Gorichev, I. G.; Izotov, A. D; Stepanov, V. M. Modeling of the effect of pH on the calcite dissolution kinetics. *Theor. Found. Chem. Eng.* **2005**, *39*, 614−621.
(27) Ruiz-Agudo, E.; Putnis, C. V.; Rodriguez-Navarro, C.; Putnis, A. Effect of pH on calcite growth at constant $a\mathrm{Ca}^{2+}/a\mathrm{CO}_3^{2-}$ ratio and supersaturation. *Geochim. Cosmochim. Acta* **2011**, *75*, 284−296.
(28) van der Weijden, R. D.; Comans, R. N. J. Sorption and sorption reversibility of cadmium on calcite in the presence of phosphate and sulfate. *Mar. Chem.* **1997**, *57*, 119−132.
(29) van Cappellen, P.; Charlet, L.; Stumm, W.; Wersin, P. A surface complexation model of the carbonate mineral-aqueous solution interface. *Geochim. Cosmochim. Acta* **1993**, *57*, 3505−3518.
(30) Pokrovsky, O. S.; Mielczarski, J. A.; Barres, O.; Schott, J. Surface speciation models of calcite and dolomite/aqueous solution interfaces and their spectroscopic evaluation. *Langmuir* **2000**, *16*, 2677−2688.
(31) Pokrovsky, O. S.; Schott, J. Surface chemistry and dissolution kinetics of divalent metal carbonates. *Environ. Sci. Technol.* **2002**, *36*, 426−432.
(32) Schott, J.; Pokrovsky, O. S.; Oelkers, E. H. The link between mineral dissolution/precipitation kinetics and solution chemistry. *Rev. Mineral. Geochem.* **2009**, *70*, 207−258.
(33) Oelkers, E. H.; Golubev, S. V.; Pokrovsky, O. S.; Bénézeth, P. Do organic ligands affect calcite dissolution rates? *Geochim. Cosmochim. Acta* **2011**, *75*, 1799−1813.
(34) Pokrovsky, O. S.; Golubev, S. V.; Jordan, G. The effect of organic and inorganic ligands on calcite and magnesite dissolution rates at 60 °C and 30 atm $p\mathrm{CO}_2$. *Chem. Geol.* **2009**, *265*, 33−43.
(35) Qiu, S. R.; Wierzbicki, A.; Orme, C. A.; Cody, A. M.; Hoyer, J. R.; Nancollas, G. H.; Zepeda, S.; De Yoreo, J. J. Molecular modulation of calcium oxalate crystallization by osteopontin and citrate. *Proc. Natl. Acad. Sci. U.S.A.* **2004**, *101*, 1811−1815.
(36) Wang, L. J.; De Yoreo, J. J.; Guan, X. Y.; Qiu, S. R.; Hoyer, J. R.; Nancollas, G. H. Constant composition studies verify the utility of the Cabrera-Vermilyea (C-V) model in explaining mechanisms of calcium oxalate monohydrate crystallization. *Cryst. Growth Des.* **2006**, *6*, 1769−1775.
(37) Tang, R. K.; Darragh, M.; Orme, C. A.; Guan, X. Y.; Hoyer, J. R.; Nancollas, G. H. Control of biomineralization dynamics by interfacial energies. *Angew. Chem., Int. Ed.* **2005**, *44*, 3698−3702.
(38) Wallace, A. F.; De Yoreo, J. J.; Dove, P. M. Kinetics of silica nucleation on carboxyl- and amine-terminated surfaces: Insights for biomineralization. *J. Am. Chem. Soc.* **2009**, *131*, 5244−5250.

(39) Himawan, C.; Starov, V. M.; Stapley, A. G. F. Thermodynamic and kinetic aspects of fat crystallization. *Adv. Colloid Interface Sci.* **2006**, *122*, 3−33.
(40) Mann, S.; Heywood, B. R.; Rajam, S.; Birchall, J. D. Controlled crystallization of $CaCO_3$ under stearic acid monolayers. *Nature* **1988**, *334*, 692−695.
(41) Mann, S.; Archibald, D. D.; Didymus, J. M.; Douglas, T.; Heywood, B. R.; Meldrum, F. C.; Reeves, N. J. Crystallization at inorganic-organic interfaces: Biominerals and biomimetic synthesis. *Science* **1993**, *261*, 1286−1292.
(42) Shin, D. W.; Ma, J. J.; Kim, D. H. The asp-rich region at the carboxyl-terminus of calsequestrin binds to Ca^{2+} and interacts with triadin. *FEBS Lett.* **2000**, *486*, 178−182.
(43) Suzuki, M.; Murayama, E.; Inoue, H.; Ozaki, N.; Tohse, H.; Kogure, T.; Nagasawa, H. Characterization of prismalin-14, a novel matrix protein from the prismatic layers of the Japanese pearl oyster (*Pinctada fucata*). *Biochem. J.* **2004**, *382*, 205−213.
(44) Elhadj, S.; De Yoreo, J. J.; Hoyer, J. R.; Dove, P. M. Role of molecular charge and hydrophilicity in regulating the kinetics of crystal growth. *Proc. Natl. Acad. Sci. U.S.A.* **2006**, *103*, 19237−19242.
(45) Piana, S.; Jones, F.; Gale, J. D. Aspartic acid as a crystal growth catalyst. *CrystEngComm* **2007**, *9*, 1187−1191.
(46) Oelkers, E. H.; Bénézeth, P.; Pokrovski, G. S. Thermodynamic databases for water-rock interaction. *Rev. Mineral. Geochem.* **2009**, *70*, 1−46.
(47) Wang, L. J.; Nancollas, G. H. Pathways to biomineralization and biodemineralization of calcium phosphates: The thermodynamic and kinetic controls. *Dalton Trans.* **2009**, 2665−2672.
(48) Zhang, J. W.; Nancollas, G. H. Kink density and rate of step movement during growth and dissolution of an AB crystal in a nonstoichiometric solution. *J. Colloid Interface Sci.* **1998**, *200*, 131−145.
(49) Perdikouri, C.; Putnis, C. V.; Kasioptas, A.; Putnis, A. An atomic force microscopy study of the growth of a calcite surface as a function of calcium/total carbonate concentration ratio in solution at constant supersaturation. *Cryst. Growth Des.* **2009**, *9*, 4344−4350.
(50) Stack, A. G.; Grantham, M. C. Growth rate of calcite steps as a function of aqueous calcium-to-carbonate ratio: Independent attachment and detachment of calcium and carbonate ions. *Cryst. Growth Des.* **2010**, *10*, 1409−1413.
(51) Larsen, K.; Bechgaard, K.; Stipp, S. L. S. The effect of the Ca^{2+} to CO_3^{2-} activity ratio on spiral growth at the calcite $\{10\bar{1}4\}$ surface. *Geochim. Cosmochim. Acta* **2010**, *74*, 2099−2109.
(52) Posner, A. S.; Betts, F. Synthetic amorphous calcium phosphate and its relation to bone mineral structure. *Acc. Chem. Res.* **1975**, *8*, 273−281.
(53) Onuma, K.; Ito, A. Cluster growth model for hydroxyapatite. *Chem. Mater.* **1998**, *10*, 3346−3351.
(54) Legeros, R. Z.; Trautz, O. R.; Legeros, J. P.; Klein, E.; Shirra, W. P. Apatite crystallites: Effects of carbonate on morphology. *Science* **1967**, *155*, 1409−1411.
(55) Dey, A.; Bomans, P. H. H.; Muller, F. A.; Will, J.; Frederik, P. M.; de With, G.; Sommerdijk, N. A. J. M. The role of prenucleation clusters in surface-induced calcium phosphate crystallization. *Nat. Mater.* **2010**, *9*, 1010−1014.
(56) Conley, D. J.; Paerl, H. W.; Howarth, R. W.; Boesch, D. F.; Seitzinger, S. P.; Havens, K. E.; Lancelot, C.; Likens, G. E. Controlling eutrophication: nitrogen and phosphorus. *Science* **2009**, *323*, 1014−1015.